REVIEW

Mid-infrared laser polarization spectroscopy for quantitative measurement of species and temperature: a review

Wanxia Zhao[1] · **Zeyad T. Alwahabi**[2] · **Bassam B. Dally**[1]

Abstract

Mid-infrared laser polarization spectroscopy (IRPS) is a powerful diagnostic technique suitable for the quantitative measurement of species concentration and temperature. IRPS is well suited to reactive multiphase flows and is not affected by the presence of particles and other nanostructures. It has the potential to detect species that have no accessible single-photon electronic transition in the UV/Visible range. In this review, an overview of the various contributions that have been devoted to the development and application of IRPS are summarized and discussed. The basic theoretical framework is presented and the nature of the IRPS experiments is described. Then, several types of IRPS applications are reviewed, including the measurement of the concentration of minor species and the temperature, the study of molecular dynamics and collision energy transfer, and the feasibility of 2D imaging with high spatial resolution. Finally, future prospects, required improvements, and potential application fields of IRPS are provided.

1 Introduction

Laser Polarization Spectroscopy (PS) is a coherent laser diagnostic technique, which allows remote detection of atoms and molecules in a harsh environment. Two laser beams are used in PS, a strong pump beam and a weak probe beam. The two beams are polarized and are aligned to cross at a spatial spot where the target molecules are present. When the wavelength of the pump laser beam is tuned to a particular molecular transition, the strong absorption will cause a birefringence effect. As the polarized probe beam passes through the same media, it will experience the generated birefringence. Using high-quality polarizers, the changes to the probe beam can be detected. As a coherent technique, PS produces a beam-like signal and it can be collected in the far-field, where the scattered light, as well as the spontaneous thermal radiation from combustion, can be

greatly suppressed. The magnitude of the effect is related to the square of the molecular concentration; hence, the signal is non-linear. In principle, two-dimensional imaging capability is possible using PS.

The first demonstration of polarization spectroscopy was performed by Wieman and Hänsch in 1976 [1]. This was introduced as a Doppler-free spectroscopic method related to saturation spectroscopy. The pump beam intensity used in PS is usually high enough to saturate the resonances that are probed to achieve a higher signal-to-noise ratio. The background noise in PS measurement can be eliminated by a pair of crossed high-quality polarizers and as such discriminate target species from the surrounding (gas, liquid) environment. In addition, compared with other nonlinear laser techniques, PS has the advantage of high intensity, and its experimental setups are relatively simple. For example, coherent anti-stokes Raman scattering (CARS) is a powerful method for monitoring species in flames [2]. However, its sensitivity is limited by the inherent non-resonant background, which makes it not applicable to detect trace species concentrations. Electronically resonant CARS and degenerate four-wave mixing (DFWM) can provide higher sensitivity than PS, but the analysis in resonant CARS is complicated, and DFWM has a problem with background scattering [3].

Similar to most laser diagnostic techniques, PS is usually applied in the UV/Visible range by exciting single-photon electronic transitions of OH [3–5], C_2 [6, 7], NH [8], NO

✉ Zeyad T. Alwahabi
zeyad.alwahabi@adelaide.edu.au

✉ Bassam B. Dally
bassam.dally@kaust.edu.sa

1 Clean Combustion Research Center, King Abdullah University of Science and Technology, Thuwal 23955-6900, Saudi Arabia

2 School of Chemical Engineering and Advanced Materials, The University of Adelaide, Adelaide, SA 5005, Australia

[9], and two-photon electronic transitions of NH_3 and CO [10]. However, only limited species can be measured in this spectral range.

Compared with laser-induced fluorescence, IRPS (and PS) detects the concentration in the ground state. It is, therefore, less affected by quenching and has the potential to be used in quantitative chemical detection. This feature permits the detection of many important species, such as CO_2, C_2H_2, and CH_4, which cannot be probed with UV/Visible PS, because they possess no accessible single-photon electronic transition in the UV/Visible range. In addition, IRPS can be used to detect molecules with a dissociated excited state "black molecule", such as C_2H.

The absence of quality infrared polarizers had delayed the demonstration of infrared laser polarization spectroscopy (IRPS) until the early 2000s. The first molecule detected by IRPS was CO_2 by Roy et al. [11], using TiO_2 polarizers with an extinction ratio of 8×10^{-5} and by Alwahabi et al. [12] using BBO polarizers with an excitement ratio of 7.1×10^{-5}. The infrared radiation reported by Roy et al. [11] was generated using an optical parametric generator pumped by a frequency-doubled Nd:YAG laser. The output radiation included two different wavelengths at 1.5 μm and 2.7 μm, where the 2.7 μm laser beam was used to probe the P(13) and P(14) resonances of the transition in CO_2. In their work, the experimental line shape showed good agreement with the numerical modeling. The line intensity for the P(14) resonance increased proportionally to the square of CO_2 number density. Alwahabi et al. [12] utilized a tunable IR laser at 2 μm, produced by an H_2-Raman shifter pumped by an Alexandrite laser, to probe the R(14) transition in CO_2.

Since then, IRPS was successfully applied in high-temperature flames to detect infrared active species, such as CH_4, CO_2, HCl, HCN, and C_2H_2, which have no conveniently accessible electronic transitions but have strong absorption in the mid-IR (2–5 um) via rovibrational transition [13]. In 2005, Li et al. [14] performed the first IRPS measurement in laminar flames to detect CO_2 and H_2O at atmospheric pressure, followed by measurements of OH and H_2O at low-pressure laminar flame [15]. In addition, IRPS has also been used to measure the temperature of minor species in flames [16]. In contrast to other coherent techniques, IRPS can provide reasonable spatial resolution to detect species with instantaneous visualization of two-dimensional distribution [4]. The application of optical diagnostics in the infra-red is usually constrained by the strong interferences from the thermal emission in flame environments. However, the coherent nature of the wave mixing process of IRPS enables it to provide excellent discrimination against background noise [17].

Recently, minor species detection based on laser techniques has been employed to study reacting flows by many

groups. The progress in this area was reviewed in detail by Kiefer and Ewart [17] with an explanation of the particular properties of each technique. Cheskis and Goldman [18] also reviewed laser-based diagnostic methods used to detect atoms and molecules at low concentrations in low-pressure flames. While the published reviews mentioned above report on the feasibility of IRPS to detect minor species in different reaction systems, none of them provides, an in-depth and comprehensive review on the application of IRPS to probe these species and the temperature.

In the present paper, we review recent works devoted to polarization spectroscopy at the mid-infrared spectral range and evaluate their findings and discoveries. The paper is arranged as follows: first, the theory of IRPS is given together with the discussion of numerical analysis of signal intensity and spectral shape, as well as the simulation of the IR spectra. Second, the experimental setup, typically used in IRPS studies, is introduced, focusing on the sources of IR generation and optical arrangement. Lastly, in Sect. 4, an up-to-date summary of the applications of IRPS for the detention of a variety of species is provided followed by insights into future prospects.

2 Theory of IR polarization spectroscopy

2.1 Numerical analysis of IRPS signals

The basic theory of PS has been discussed earlier by Demtröder [19] and Teets et al. [20], while here we provide details of the technique noting important features and practical considerations. Under PS, the linearly polarized probe always contains the propagating right (σ^+) and left (σ^-) circularly polarized components. After passing a path length (L), these two components can be written as:

$$E^+ = E_0^+ e^{i\left[\omega t - k^+ L + i\left(\frac{\alpha^+}{2}\right)L\right]} \tag{1}$$

$$E^- = E_0^- e^{i\left[\omega t - k^- L + i\left(\frac{\alpha^-}{2}\right)L\right]}, \tag{2}$$

where α^+ and α^- are absorption coefficients; n^+ and n^- are refractive indices; ω is the laser frequency. When passing the intersection region of the pump beam and the probe beam, a phase difference

$$\Delta\phi = \left(k^+ - k^-\right)L = \left(\frac{\omega L}{c}\right)\Delta n \tag{3}$$

develops with a small difference in amplitude:

$$\Delta E = \frac{E_0}{2}\left[e^{-\left(\frac{\alpha^+}{2}\right)L} - e^{-\left(\frac{\alpha^-}{2}\right)L}\right]. \tag{4}$$

For most practical cases, the difference in absorption coefficient ($\Delta \alpha = \alpha^+ - \alpha^-$) and refractive index ($\Delta n = n^+ - n^-$) are much less than 1. Assuming the laser pulse duration and lifetime of the excited state are short, and the repopulation of the initial energy state due to fluorescence and quenching is neglected [17], the transmitted intensity can be written as:

$$I_t = I_0 \left[\xi + \theta^2 + \left(\frac{1}{2} \Delta a_w \right)^2 \right. \\ \left. + \frac{1}{4} \Delta a_w \Delta \alpha L + \frac{\omega}{c} \theta L \Delta n + \left(\frac{\omega}{2c} L \Delta n \right)^2 + \left(\frac{\Delta \alpha L}{4} \right)^2 \right], \tag{5}$$

where I_0 is the incident probe intensity; ξ is the leakage through the crossed polarizers; L is the probing length; θ is the angular deviation from the ideal crossing angle of the polarizers; a_W is the absorption in the two windows of the apparatus.

After introducing the parameter b to express the additional birefringence effects ($\frac{1}{2} \Delta a_w$), which are contributed by the absorption of optical components, for example, the windows between polarizers, the line profile for the circularly polarized pump beam, I_{PS}, can be written as:

$$I_{IRPS} = I_0 \left[\xi + \theta^2 + (b)^2 + \frac{1}{2} bL(\Delta \alpha) \right. \\ \left. + \theta L \left(\frac{\omega \Delta n}{c} \right) + \left(\frac{\omega L}{2c} \Delta n \right)^2 + \left(\frac{\Delta \alpha L}{4} \right)^2 \right]. \tag{6}$$

The line profile of $\Delta \alpha(\omega)$ can be expressed as a Lorentzian profile:

$$\Delta \alpha(\omega) = \frac{\Delta \alpha_0}{1 + x^2} \tag{7}$$

$$x = \frac{\omega_0 - \omega}{\frac{\gamma_s}{2}}, \tag{8}$$

where γ_s is the halfwidth; ω_0 is the center frequency and $\alpha_0 = \alpha(\omega_0)$. In addition, the difference in the refractive index, Δn, is related to, $\Delta \alpha$, by Kramers–Kronig relation [1] as:

$$\Delta n(\omega) = \frac{c}{\omega_0} \frac{\Delta \alpha_0 x}{1 + x^2}. \tag{9}$$

For some specific cases where there are no additional optical components between the polarizers, or the polarizers are inside the chamber, parameter b can be neglected. In addition, θ can also be neglected when the alignment of the polarizers is optimum. Therefore, substituting Eqs. (7)–(9) into Eq. (6), the simplified equation can be written as:

When only considering the transition that is close to the center frequency, where $\omega - \omega_0$ is close to zero, Eq. (10) can be further simplified to:

$$I_{IRPS} = I_0 \left[\xi + \left(\frac{\Delta \alpha_0 \cdot L}{4} \right)^2 \right]. \tag{11}$$

Taking the geometry factor of the pump beam involved, the difference in absorption coefficient for a molecular transition (J, M) to (J', M $\pm$ 1) can be expressed:

$$\Delta \alpha_0 = \sum_M N_M \left(\sigma_{JJ',M}^+ - \sigma_{JJ',M}^- \right). \tag{12}$$

That is,

$$\Delta \alpha_0 = - \frac{N_0 \cdot \sigma_{JJ'} \cdot I_{pump} \cdot \xi_{JJ'}}{S}, \tag{13}$$

where $\sigma_{JJ'}$ is the polarization-independent absorption cross-section; N_M refers to the population of the magnetic sublevels; N_0 is the initial state population of the detected molecules; I_{pump} is the pump intensity; $\xi_{JJ'}$ is the polarization numerical factor that takes the angular momenta of the energy states into account; S is the saturation parameter, which depends on dephasing rate, collisional quenching, pump beam intensity, and transition probability. [21]

Therefore, Eq. (11) can be rewritten as:

$$I_{IRPS} = AI_0 \left[\xi + \left(\frac{N_0 \cdot \sigma_{JJ'} \cdot I_{pump} \cdot \xi_{JJ'} \cdot L}{4S} \right)^2 \right], \tag{14}$$

where A is the scaling factor. The numerical values of $\xi_{JJ'}$ for P, Q, and R transitions are also deduced by Demtröder [19] and indicate that high signal intensities can be generated using linearly polarized pumping for Q-branches and circularly polarized pumping for P- and R-branches. The relationship between $\xi_{JJ'}$ and the rotational quantum number, J, for P, Q, and R transitions proposed by Demtröder [19], is presented in Fig. 1.

Saturation effects play a crucial role in PS molecular transitions. Under high-temperature flames, the Doppler broadening dominates the linewidth and the signal intensity in an unsaturated regime and a saturated regime can be written as: [22, 23]

$$I_{IRPS}^{Unsaturated} \propto I_{pump}^2 \cdot I_{probe} \cdot \left(\frac{1}{\Delta \omega_D} \right)^2 \cdot \left(\frac{1}{\Delta \omega_C} \right)^4 \tag{15}$$
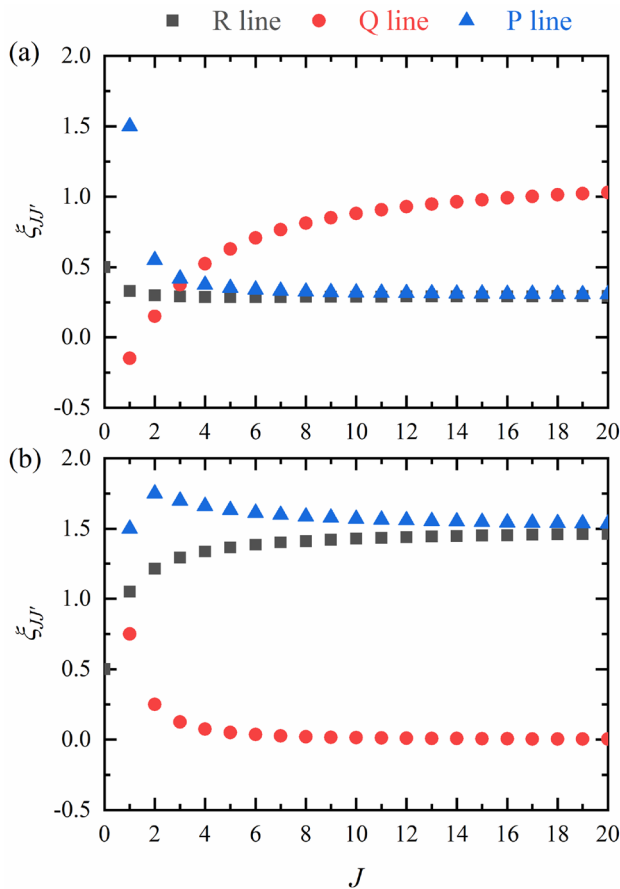
$$I_{IRPS} = I_0 \left[\xi + \left(\frac{\omega \cdot L \cdot \Delta \alpha_0}{2 \omega_0} \right)^2 \cdot \left(\frac{x}{1 + x^2} \right)^2 + \left(\frac{\Delta \alpha_0 \cdot L}{4} \right)^2 \cdot \left(\frac{1}{1 + x^2} \right)^2 \right]. \tag{10}$$

Fig. 1 The polarization numerical factor gives the J dependence on **a** linearly and **b** circularly polarized light. [19]

$$I_{IRPS}^{Saturated} \propto I_{probe} \cdot \left(\frac{1}{\Delta\omega_D}\right)^2 \cdot \left(\frac{1}{\Delta\omega_C}\right)^{<1}, \tag{16}$$

where $\Delta\omega_C$ and $\Delta\omega_D$ are the collisional broadening width and the Doppler width, respectively. Comparing Eqs. (15) and (16), the PS signal is only dependent on the probe beam intensity under the saturating conditions. In many cases, the saturating conditions are usually selected to perform the experiments because of the low effect of intensity fluctuations and high signal intensity when using high pump energy.

Additionally, the signal-to-noise (S/N) ratio of PS can be estimated by

$$\frac{S}{N} = a\frac{\theta \cdot \alpha_0 \cdot L \cdot S_0}{\xi + \theta^2}\xi_{JJ'}, \tag{17}$$

where a is a factor of the intensity stability of the probe beam. Its value is determined by the crossing angle (θ) of

two polarizers and achieves the maximum as below when $\theta^2 = \xi$.

$$\left(\frac{S}{N}\right)_{max} = a\frac{\alpha_0 \cdot L \cdot S_0}{2\sqrt{\xi}}\xi_{JJ'}. \tag{18}$$

Compared to other saturation spectroscopy, whose S/N ratio is

$$\frac{S}{N} = \frac{1}{2}a \cdot \alpha_0 \cdot L \cdot S_0. \tag{19}$$

The S/N ratio of polarization spectroscopy can be increased by the factor of $\xi_{JJ'}/\sqrt{\xi}$. For example, if $\xi_{JJ'} = 0.5$, $\xi = 10^{-6}$, the S/N ratio of PS is 500 times higher than saturated absorption spectroscopy [19].

In addition, because the S/N ratio is a function of ξ, highly sensitive PS detection can be achieved by choosing a pair of polarizers with a low extinction ratio (for example 10^{-6}). Worth noting that such polarizers are easier to manufacture in the IR range, because the scattering caused by material impurities and surface flatness in the IR range is much less than that in the UV/Vis range [21].

As high PS signal intensity and S/N ratio can also be achieved by using a pump beam with high energy to reduce intensity fluctuations, Li et al. [15] used the equation:

$$I_{IRPS} \propto I_{laser} \cdot \xi_{JJ'}^2 \cdot N_0^2 \cdot B^2 \tag{20}$$

to simulate the saturation condition of the mid-IRPS signal, where B is the Einstein coefficient. It is noted that the leakage through the crossed polarizers is neglected in Eq. (20). In another work reported by Sun et al. [24], after taking the collision effect at different conditions into consideration, they expressed the saturated IRPS signal as

$$I_{IRPS} = A \cdot I_{laser} \cdot g \cdot c \cdot \xi_{JJ'}^2 \cdot N_0^2 \cdot \sigma^2. \tag{21}$$

Sun et al. [24] introduced two new parameters: g is a parameter accounting for the spectral overlap between laser beam profile and the absorption profile of the molecular line and c is a parameter accounting for the collision effects under different conditions, including temperature, pressure, and buffer gas/es. Using the same optical setup, the parameters A, $\xi_{JJ'}$, and I_{laser} were assumed to be unchanged for the same transition.

According to Eq. (20) and (21), the signal intensity of IRPS depends quadratically on the population distribution of the lower states of the probed transition. Compared to linear absorption techniques, the strong enhanced lines in PS can provide a higher spectral resolution. By manipulating the polarization status of the pump beam linearly or circularly,

the Q-, R-, and P-branches can be selectively enhanced, which has the potential to simplify the measurement of temperatures and species concentrations.

Furthermore, in the work reported by Alwahabi et al. [25], with the polarizers are perfectly crossed, the IRPS signal can be expressed as

$$I_{IRPS} \cong I_{probe}\left(\xi + \left(\frac{\Delta\alpha l}{4}\right)^2 G(\omega)\right) \tag{22}$$

$$\Delta\alpha = N \cdot f_B \cdot \sigma^2 \cdot \frac{I_{pump}\tau_{pump}}{\hbar\omega} \cdot \xi_{JJ'}, \tag{23}$$

where $G(\omega)$ is the normalized line shape of the species absorption function; $\Delta\alpha$ is the induced dichroism; N is the number of molecules or radicals; f_B is the Boltzmann fraction. The term, f_B, can be expressed with rotational energy levels, E_J, as:

$$f_B = (2J+1)e^{-\frac{E_J}{kT}}, \tag{24}$$

where J is the total rotational quantum number, k is the Boltzmann constant, and T is the gas temperature.

According to Banwell [26], the spectral intensities are proportional to the initial numbers of molecules in each energy level. The first factor governing the molecular population is the Boltzmann distribution. The molecules distributed between the two states are:

$$\frac{N_2}{N_1} = e^{-\frac{E_2 - E_1}{kT}}. \tag{25}$$

The second factor is the possibility of degeneracy in the energy states, $2J+1$. Therefore, although the molecular population in each energy level decreases exponentially in Eq. (25), the degeneracy in the energy levels increases with J. Combining the Boltzmann distribution and the degeneracy, the total population at an energy E_J can be written as:

$$Population \propto (2J+1)e^{-\frac{E_J}{kT}} \tag{26}$$

which has been considered as Boltzmann fraction in Eq. (24).

To demonstrate the line shapes of PS signals, Wieman and Hansch [1] first reported that the shapes are Lorentzian when the Doppler width is greater than the collision width, whereas Demtroder [19] assumed that the PS line shapes are always Lorentzian. Reichardt and Lucht [23] reported a theoretical calculation of line shapes in polarization spectroscopy. They found that at the low pump laser energy, the PS line shape was Lorentzian-cubed for a homogeneously broadened resonance, as compared to the Lorentzian predicted in previous works.

The normalized Lorentzian profile can be written as:

$$L(\omega - \omega_0) = \frac{\frac{\gamma}{2\pi}}{(\omega - \omega_0)^2 + \left(\frac{\gamma}{2}\right)^2}, \tag{27}$$

where ω is the laser wavelength in cm^{-1}, γ is the full width at half-maximum (FWHM) [19]. Considering pressure and temperature conditions, Alwahabi et al. [25, 27] measured the pressure broadened normalized Lorentzian-cubed profile, for CO_2, using:

$$g(\omega) = \frac{1}{1 + \left[\frac{2(\omega - \omega_0)}{\Delta\omega_n + \Delta\omega_{self} + \Delta\omega_{foreign}}\right]^3}, \tag{28}$$

where $\Delta\omega_n$ is the natural linewidth, $\Delta\omega_{self}$ and $\Delta\omega_{foreign}$ are the line broadening due to the self and the buffer gas collisions, respectively. At the pressure above a few millitorrs, collision broadening is much greater than the natural linewidth [28].

2.2 Spectra simulation

By taking the population of states and line shapes into account, the IRPS signal intensity can be calculated using the following equations with the term of temperature, T:

$$IRPS \propto \left(\frac{A_{JJ'} \cdot NSS \cdot (2J+1)e^{-\frac{E_J}{kT}}}{Q(T)}\right)^2 \cdot \xi_{JJ'}^2 \tag{29}$$

$$L(\omega) = I_{IRPS} \cdot \frac{\frac{\gamma}{2\pi}}{(\omega - \omega_0)^2 + (\gamma/2)^2}, \tag{30}$$

where $Q(T)$ is the total internal partition sum for infrared absorbing molecules, and $A_{JJ'}$ is the Einstein A-coefficient. Three factors were introduced in the equation, which are Boltzmann fraction (f_B), nuclear spin statistics (NSS), and polarization numerical factor ($\xi_{JJ'}$). All lines are characterized by a Lorentzian profile in the simulation.

In addition, the HITRAN database is a well-known spectroscopic database to provide necessary information about the transmission and emission of large molecules in the atmosphere and help with the identification of transition lines. Taking acetylene (C_2H_2) as a typical example, Fig. 2 shows the simulated partial IRPS spectrum of C_2H_2 at room temperature for the transitions of P(10) to P(15) and R(10) to R(15). The parameters of line position and intensity are directly extracted from the HITRAN database [29]. Then, a Lorentzian function, which is shown in Eq. (30), is used to characterize
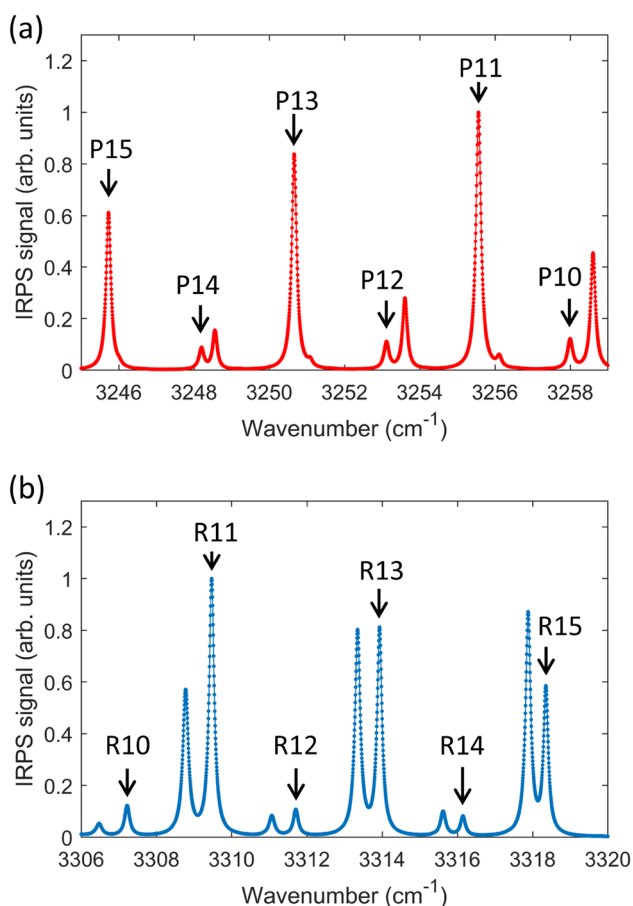
Fig. 2 The simulated partial IRPS spectra of C_2H_2 at room temperature for the transitions of **a** P(10) to P(15) and **b** R(10) to R(15). The parameters of line position and signal intensity are directly extracted from the HITRAN database. The line profiles were characterized by a Lorentzian profile

3 Experiment of IR polarization spectroscopy

3.1 IR sources in polarization spectroscopy

For continuous-wave tunable IR radiation, quantum cascade lasers are readily available [31, 32]. There are a few methods to generate tunable pulsed IR, these are single-longitudinal-mode (SLM) pulsed alexandrite ring laser [12], optical parametric generator (OPG) [11], and non-linear crystals [32, 33] pumped by Nd:YAG laser. In quantitative species measurement in flames, coherent IR light is mainly produced based on the difference-frequency generation of visible sources in non-linear crystals [32]. In detail, an injection-seeded Nd:YAG laser is used to pump a tunable dye laser. The output of the dye laser is then mixed with part of the fundamental infrared output of the Nd:YAG laser in a crystal to generate a tunable pulsed IR laser beam. As it is difficult to calibrate the solute concentration of an open shell chemical species (radical), tunable IR lasers offer the advantages for detecting closed-shell molecules in the electronic ground state and eliminate the requirement of convenient electronic transitions. For example, Li et al. [34] mixed a part of the fundamental 1064 mm Nd:YAG beam with a dye-laser beam in a $LiNbO_3$ crystal. A tunable IR laser beam was subsequently generated at the wavelength around 3 μm.

Although tunable lasers can only be tuned within a relatively narrow range of wavenumbers, they are still promising if the IR signature of the adsorbed species is well established. In such cases, light absorption can be focused on a certain frequency or a narrow range of frequencies. The IR absorption can be obtained directly within a given region without the requirement of recording the full spectra or carrying out Fourier transformations.

3.2 Typical setup arrangement for IRPS

Figure 3 shows a typical optical setup for collecting IRPS signals from gaseous species in flames. A weak linearly polarized probe beam is crossed with a strong linearly or circularly polarized pump beam to define an interaction volume. The optical pumping of the target species with the polarized pump beam produces birefringence and induces detectable polarization changes in the weak probe beam [10]. The pump beam and probe beam have the same frequency, which is close to a resonant molecular transition.
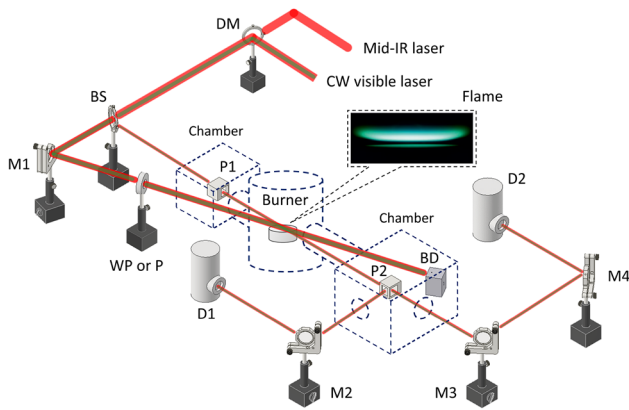
the line profile. The spectra are simulated at room temperature. Due to the symmetric structure of the C_2H_2, the nuclear spin statistics for even J states for C_2H_2, is 1, while for odd J states it is 3 [30]. It introduces an enhancement in the PS signal intensity by a factor of 9. Therefore, the spectrum intensities for $J =$ odd are significantly higher than that for $J =$ even. The specific lines in the simulated IRPS spectra can be further selected to identify and evaluate the target species in the experiment. For example, Sun et al. [24] chose P(13) and P(19) as two candidate lines, which have strong intensity at room temperature and in sooty flames with weak interference, while Li et al. [21] selected the P(11) line for a detailed IRPS investigation of C_2H_2.

Fig. 3 Experimental setup of IR polarization spectroscopy for the detection of gas species. DM: dichroic mirror; BS: beam splitter; P: polarizer; D1: detector for the absorption measurements; D2: detector for the IRPS signal; WP: waveplate; M: mirror; BD: beam dump; The inserted photo shows the dimethyl ether/O_2/Ar flame at 37 mbar [16]

The detection volume (DV) of the measurement is identified by the interaction volume between the crossed pump beam and probe beam. Table 1 shows typical examples of the interaction volume with the crossing angle, θ, from $0°$ to $90°$. The pump beam is indicated in red color, while the probe beam is indicated in yellow color. The detection volume can be calculated by the integral for the common volume of two cylindrical beams using the following equation:

$$V\left(r_1, r_2, \theta\right) = \frac{8}{\sin\theta} \int_0^{r_1} \left(r_2^2 - x^2\right)^{\frac{1}{2}} \cdot \left(r_1^2 - x^2\right)^{\frac{1}{2}} dx, \qquad (31)$$

where r_1 and r_2 are the radii of two crossed beams. The detection volume presents a strong dependence on the crossing angle, which is usually adjusted for different cases to achieve desired spatial resolution and signal intensity. In most experiments, the crossing angle is less than $10°$ to achieve a large detection volume and sufficient signal intensity [10].

In addition, the detection length (DL) is defined as the interaction path along with the probe beam. Its value also decreases with the increasing crossing angle. As shown in Table 1, at $\theta = 0°$, two beams are overlapped, and the detection length tends to infinity, while at $\theta = 90°$, the detection length decreases to the minimum value, which equals the diameter of the pump beam. The dependence of detection length on the crossing angle and the diameter of the pump beam, d_{pump}, can be expressed as:

$$DL = \frac{d_{pump}}{\sin\theta}. \qquad (32)$$

Because the diameter of the laser beam is in the millimeter range, the length of the interaction volume is usually approximately a few millimeters.

A uniaxial gas model of the geometrical dependence of polarization spectroscopy has been described by Reppel and Alwahabi [35]. The model provides theoretical expression describing the signal intensity as a function of

Table 1 Illustration of the interaction volume between two crossed beams with the crossing angle, θ, of (a) 0°, (b) 15°, (c) 30°, and (d) 90°. At θ=0°, two beams are overlapped, and the detection length tends to infinity, while at θ=90°, the detection length is equal to the diameter of the focused pump beam at the intersection point. The crossing angle is usually less than 10° in the experiments to achieve a large detection volume and sufficient signal intensity

θ (°)	Detection Volume (DV)	Detection Length (DL)	
		Shape	Value
0			∞
15			$3.86\ d_{pump}$
30			$2\ d_{pump}$
90			d_{pump}

the probe-pump interaction geometry. When the polarizers are perfectly crossed, the geometrical dependence of PS for linearly polarized pump beam is:

$$F_{lin}(\gamma, \kappa, \chi) = \frac{\left(\sin(2\gamma)\left(cos^2(\kappa) - sin^2(\kappa)cos^2(\chi)\right) - \cos(2\gamma)\sin(2\kappa)\cos(\chi)\right)^2}{sin^2(\chi)\left(1 - sin^2(\kappa)sin^2(\chi)\right)} \tag{33}$$

while for circularly polarized pump beam, it is:

$$F_{circ}(\gamma, \chi) = sin^2(2\gamma)sin^2(\chi)\left(\frac{\Delta + \sigma^2}{2}\right)^2, \tag{34}$$

where σ is the maximum induced circular birefringence, $\Delta/2$ is the maximum induced linear dichroism, χ is the intersection angle of the probe and pump beams, γ is the angle between the probe beam polarization direction and the vertical axis, and κ is the angle between the pump beam polarization direction and the vertical axis. These expressions are particularly useful when polarization spectroscopy is used in imaging applications.

The polarization of the pump beam can be set to either linear or circular using a half-wave- or a quarter-wave-plate, respectively. Furthermore, to visualize the IR beam and facilitate alignment, the IR beam is usually overlapped with a visible He–Ne laser. The IRPS technique has the unique ability to distinguish spectral transitions belonging to P, R, or Q branches by analyzing the J-dependence of the polarization cross-sections [36].

At atmospheric pressure, the IRPS signal intensity can be influenced significantly by different buffering gases and result in large uncertainty in concentration due to the collision effect. To improve the measurement accuracy, low-pressure conditions can be applied to minimize the collision effect. In addition, the IRPS signal strength can also be influenced by other parameters, for example, the incorrect alignment of the polarizers, laser shot-to-shot variation, particle scattering, turbulent-induced anisotropy, and beam steering, when IRPS is applied in non-isothermal conditions. Careful regular inspection of the polarizers' orientation is essential. To account for the laser shot-to-shot fluctuations, it is useful to record the energy of each laser shot using a pickup window with an IR detector. The recorded IRPS signal can be either corrected or sorted, based on the laser energy. The beam steering issue can influence the IRPS significantly if it is not taken into consideration. The pointing direction of the laser beam may change after having passed through local thermal gradients, such as those in flames and plasma. Beam steering in the vertical direction will cause the loss of the signal, while beam steering in the horizontal direction will change the value of the crossing angle between the two beams. It is useful to record the spatial location of the pump beam for future conditional IRPS data processing.

Lucas et al. [37] studied the effect of the UV beam steering in a welding plasma environment. They found that there is a maximum unavoidable error of ~ 2%. It is worth mentioning that the effect of beam steering is less severe for the IR compared to the UV wavelength. The same is true for the laser scattering as it scales to the l^4. The topic of turbulent-induced anisotropy is yet to be investigated.

A sensitive detector, such as indium-antimonide (InSb), is usually selected to improve the S/N ratio, which is especially important for the minor species with low concentration. The interference from birefringence in the windows can be avoided by placing the polarizers inside the low-pressure chamber. As a large extinction ratio of the polarizer can reduce the sensitivity of PS detection, a pair of polarizers with a low extinction ratio (for example 10^{-6}) is also significant in the measurement. In addition, the laser instabilities may cause the fluctuation of the detected signal. To eliminate this effect, two detectors can be applied before and after the detection volume to monitor the change between laser power and IRPS signal simultaneously.

4 Quantitative detection of species and temperature using IRPS

Infrared polarization spectroscopy has been employed to quantitatively measure gaseous species in flames. As most molecules possess infrared-active vibrational transitions, the detection in the mid-IR range provides great advantages for reactive scalars, especially for the molecules that cannot be accessed via the electronic transition, such as H_2O, CO_2, and CH_4.

The first experiment to detect hot nascent species of CO_2 and H_2O in flame, using the mid-IR spectral range at atmospheric pressure was conducted by Li et al. [14]. The IR beam was generated at the wavelength of 2.7 μm with an FWHM laser linewidth of 0.025 cm^{-1}. The lines belonging to CO_2 (~ 3695.2 cm^{-1}) and H_2O (~ 3696.9 cm^{-1}) were recognized in the chosen spectral region to avoid spectral interferences. Moreover, they reported further work on OH and hot water detection in low-pressure flames [15]. Rotational lines of OH radicals were assigned among hot water lines. Sensitive detection of OH at flame conditions was conducted with a high S/N ratio (> 1000:1). This study proved the applicability of IRPS in detailed flame chemistry investigation, especially for detecting minor species and eliminating interferences in reacting flows.

Recently, infrared polarization spectroscopy has been also applied to detect hydrocarbon molecules [17]. The C-H asymmetric stretching in such species typically occurs around 3000 cm^{-1}. For example, CH_4 diluted with Ar was detected in the mid-IR spectral region [38]. The spectra of P, Q, and R branches were recorded using linearly and circularly polarized pump beams. Richard and Ewart [39] recorded the PS signals of CH_4 at the pressure around 5 Torr and compare its S/N ratio with the spectra obtained using infrared degenerate four-wave mixing (IR-DFWM) spectroscopy. Furthermore, Sun et al. [22] performed quantitative measurements to study the influences of the equivalence ratio (Φ) and the height above burner (HAB) on C_2H_2 signals in the buffer gases of N_2 and CO_2 [24] as well as HCN signals in $CH_4/N_2O/O_2/N_2$ flames [40, 41]. Both collision effects and the spectral overlap factor were taken into consideration in the calibration process. Their experimental results showed a good agreement with the simulation spectra. More recently, by probing the C-H asymmetric stretching in the spectral range of 2970–3340 cm^{-1}, Sahlberg et al. [16] demonstrated the non-intrusive detection of C_2H_6, C_2H_2, and CH_4 in the low-pressure flame. The collision effects on the IRPS signal were reported at sub-atmospheric pressure of 37 mbar. Pedersen et al. [42] collected the IRPS signal of CH_4 in an N_2 flow and compared the S/N ratio obtained using an InSb photodiode and using an upconversion detector.

Table 2 provides a summary of the various reported studies on the detection of combustion species employing IR polarization spectroscopy.

In order to indicate the possibility of quantitative measurements using IRPS, the signal intensity as a function of the molecular concentration has been demonstrated for different minor species and high spatial resolution. The PS signal usually depends quadratically on the concentration. For example, Roy et al. [11] first reported the line-integrated PS signal as a function of the number density of the CO_2 molecule for the P(14) resonance. The PS signal is proportional to the square of the molecular concentration. The fluctuation of the data points was caused by the different collisional rates between CO_2 and the buffer gas of Argon. After that, Li et al. [34] estimated the relationship between the IRPS intensity and the HCl concentrations in flames. They used a quadratic function to fit the data points and obtained a detection limit of 50 ppm, which has a good agreement with the common PS theory. Additionally, Li et al. [38] reported a linear dependence of IRPS signals on CH_4 mole fraction in another study. The slope of the linear fit was 1.1 with the CH_4 mole fraction lower than 3.56%. Different from the generally expected quadratic dependence mentioned above, the linear relationship reported in this work may be caused by the absorption of the probe beam and the relatively lower number density of CH_4 in the probed volume due to gas diffusion in the gas jet [38]. Fig. 4 summarizes the dependence of IRPS signal on molecular concentrations for commonly detected species in flames.

In addition, IRPS is an attractive tool to study molecular dynamics and collision energy transfer. This is because the time scale of the measurement is given by the overlap pump and probe beams' pulse length, which is short and may be adjusted by the time delay of one beam with respect to the other. Figure 5 shows short IRPS scans near the absorption frequency of C_2H_2 P(11), namely at 3255.5615 cm^{-1}. Each scan was recorded with a binary mixture of C_2H_2 and Kr, under low pressure and ambient temperature conditions. In each scan, the C_2H_2 pressure was kept constant at 74.5 mTorr and the Kr pressure was increased from 6 to 130 Torr. As the pressure increases, the IRPS signal decrease reaching a small value, following the collision rate constant. For quantitative detection evaluation, the collisional rate constant becomes important.

On the other hand, IR polarization spectroscopy has the capability to be used as a tool to determine the temperatures of combustion species under low-pressure flames. In 2019, Sahlberg et al. [16] investigated flame temperature via recording the line ratios of hot water around 3.1 μm. In their work, the H_2O spectral line was selected, because its state energy difference is less sensitive to the changes in flame temperature. Additionally, its line strength can be neglected at room temperature, which is important to avoid interference from laser absorption in the ambient air. As shown in Fig. 6a, the line ratios of H_2O lines were sensitive to the temperature change between 1000 and 2500 K. Their work proved the great promise of this technique in the application of in situ and non-intrusive temperature measurement in low-pressure flames.

In contrast to other coherent techniques, polarization spectroscopy can be extended from point measurement to planar measurement, which allows the instantaneous two-dimensional (2D) imaging of combustion species with high spatial resolution [17]. For example, Sun et al. demonstrated the capability of IR polarization spectroscopy for instantaneous and planar imaging of HF molecules in a flame as shown in Fig. 6b [46]. Using the excitation of R(3) and R(9) lines, the imaging of HF molecule was demonstrated in CH_4 and O_2 mixed flame. In principle, 2D temperature imaging can be derived from two IRPS images by overlapping them pixel by pixel. High spatial and temporal resolution make this technique highly attractive in turbulent flows. However, because of the low S/N ratio and the absence of absorption cross-section values for the hot line transition, the 2D temperature measurement has not yet been reported extensively in the literature [46].

Although, in principle, it is possible to record the IRPS signal of two (or more) ro-vibrational transitions and then relate the IRPS intensity to the ground-state-population, it is

Table 2 Detected molecules and radicals of gases in combustion flames using IR polarization spectroscopy

Radicals / molecules	Wavenumber (cm^{-1})	Resonance	IR light source	Type of polarizers/ Extinction ratio	Crossing angle (°)	Pressure (mbar)	Temperature (K)	Comment	Ref
CO_2	4988	R(14)	Injection seeded single-longitudinal-mode (SLM) pulsed alexandrite ring laser system	Beta barium borate (BBO) polarizers / 7.1×10^{-5} Calcite polarizer	7	Atmospheric pressure	Ambient temperature	Obtained the pressure broadening coefficients of CO_2 by Ar, He, and N_2 at atmospheric pressure The IRPS behavior appears to be insensitive to the inter- and intra- vibrational energy transfers	Alwahabi 2004—2007 [12, 25, 27]
	3698–3699	P(13), P(14)	Optical parametric generator (OPG) pumped by Nd:YAG laser	TiO_2 polarizers / 8×10^{-5}	7	Atmospheric pressure and 160	Ambient temperature	FWHM: 0.09 cm^{-1} Measured the number density of CO_2 as a function of the PS signal strength for P(14) resonance	Roy 2002 [11]
	2310	P(30)	CW distributed feedback quantum cascade laser	Wire-grid polarizers / 1×10^{-2} High extinction-rate polarizer / 1.6×10^{-5}	2	0.02 to 0.1 for pure CO_2	Ambient temperature	Obtained a high S/N ratio (250) using double-balanced detection	Bartalini 2009 [32]
	3695.2464	P(32)	LiNbO$_3$ crystal pumped by Nd:YAG and dye laser	YVO4 IR polarizers / 6×10^{-8}	6.5	Atmospheric pressure	Assuming 1800 for all flames	Obtained line integrated IRPS signal versus CO_2 number density	Li 2005 [14]
C_2H_2	3226 3223	P(23) P(24)	LiNbO$_3$ crystal pumped by Nd:YAG and dye laser (Styryl 11 dye)	YVO4 IR polarizers / 6×10^{-8}	6.5	22.5 to 82 and atmospheric pressure	Assuming 1800	Detection limit: 30 ppm (1 atm), 10 ppm (70 mbar)	Li 2007 [21]
	3250.7 3248.5	P(13) P(19)		YVO4 IR polarizers	3	Atmospheric pressure	Up to 1750	C_2H_2 mole fraction increased to 0.035 ($\Phi = 2.50$ C_2H_4/air flame, HAB $= 8.5$ mm)	Sun 2010 [24]
	3331–3336	R(21)–R(23)	LiNbO$_3$ crystal pumped by Nd:YAG and dye laser (Styryl 9 dye)	YVO4 IR polarizers	4	<Atmospheric pressure	1088	Detection limit: 400 ppm (37 mbar)	Sahlberg 2019 [16]

Table 2 (continued)

Radicals / molecules	Wavenumber (cm^{-1})	Resonance	IR light source	Type of polarizers/ Extinction ratio	Crossing angle (°)	Pressure (mbar)	Temperature (K)	Comment	Ref
CH_4	2968	P(5)	LiNbO$_3$ crystal pumped by Nd:YAG and dye laser (Styryl 9 dye)	YVO4 IR polarizers / 6.6×10^{-7}	6.3	Atmospheric pressure	Ambient temperature	S/N ratio > 10^4 Detection limit: 100 ppm (1 atm)	Li 2004 [38]
	3148–3166	R(13)–R(15)	YVO4 IR polarizers		4	37 to 1013	300 to 1600	Detection limit: 1900 ppm (37 mbar) CH$_4$ mole fraction increased to 0.37 (Φ=1.87 DME/O$_2$/Ar flame, 37 mbar, HAB=2.5 mm)	Sahlberg 2019 [16]
	3148.8	R(13)		—	3.9	Atmospheric pressure	Ambient temperature	Obtained a factor 64 improvement in the SNR using an upconversion detector	Pedersen 2018 [42]
	3018.3585	Q(3)	Frequency-doubled, seeded single-mode, Nd:YAG laser	YVO4 IR polarizers / 2.6×10^{-7}	—	6.7 for pure CH$_4$	Ambient temperature	S/N ratio = 110 with CH$_4$ pressures of >1 Torr Pressure broadening = 6.3 ± 1.5 MHz Torr^{-1}	Richard and Ewart 2009 [39]
HCl	3030–3073 (HCl^{35}) 3028–3071 (HCl^{37})	R(7)–R(10) R(7)–R(10)	LiNbO$_3$ crystal pumped by Nd:YAG and dye laser (Styryl 11 dye)	YVO4 IR polarizers	2.8	Atmospheric pressure	Simulated water lines at 2000	S/N ratio = 10, detection limit: 50 ppm Dependence of the HCl signal intensity on HCl concentration was observed	Li 2008 [34]
	—	—			2.2	Atmospheric pressure	943 to 1023	In situ measurements of the concentration of HCl in a tube furnace	Sun 2011 [43]
HCN	3252.4 3248.5	P(19) P(20)	LiNbO$_3$ crystal pumped by Nd:YAG and dye laser (Styryl 11 dye)	YVO4 IR polarizers	2.2	Atmospheric pressure	Up to 2000	Axial profiles of HCN measured in three rich CH$_4$/N$_2$/O$_2$/N$_2$ flames (Φ=1.6, 1.4, 1.2 HAB=3–10 mm)	Sun 2011 [40]
	—	—			6.5	Atmospheric pressure	1023 and 1223	In situ measurements of the concentration of HCN in a tube furnace High temperatures and good ventilation conditions result in high concentrations	Sun 2011 [41]
OH	3199–3333	P(6)–P(9)	LiNbO$_3$ crystal pumped by Nd:YAG and dye laser (Styryl 11 dye)	YVO4 IR polarizers / 6×10^{-8}	6.5	39 to 47	1000 to 2050	A high S/N ratio (> 1000:1) indicates the feasibility of mid–IRPS OH detection	Li 2007 [15]
	—	P(11)	Distributed–feedback dye lasers pumped by Nd:YAG	BBO polarizers	2	Atmospheric pressure	Around 2000	Measurement of rotational energy transfer and collisional dynamics such as realignment, reorientation	Chen 2004 [44]

Fig. 4 IRPS signal intensity as a function of the species concentrations for **a** CO_2; Reproduced from ref. [14] with permission. Copyright 2005 Elsevier; **b** C_2H_2; Reproduced from ref. [21] with permission. Copyright 2007 Elsevier; **c** HCl; Reproduced from ref. [34] with permission. Copyright 2008 The Optical Society; and **d** CH_4. Reproduced from ref. [38] with permission. Copyright 2004 Springer
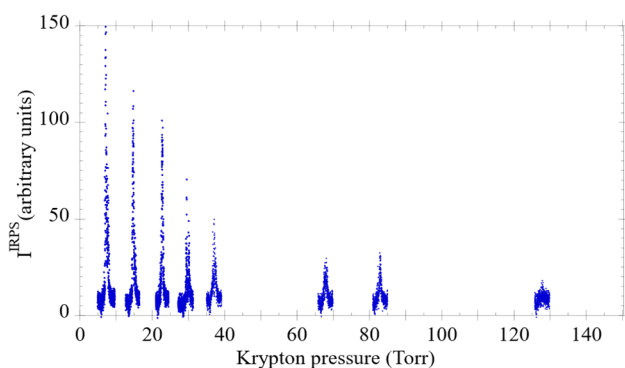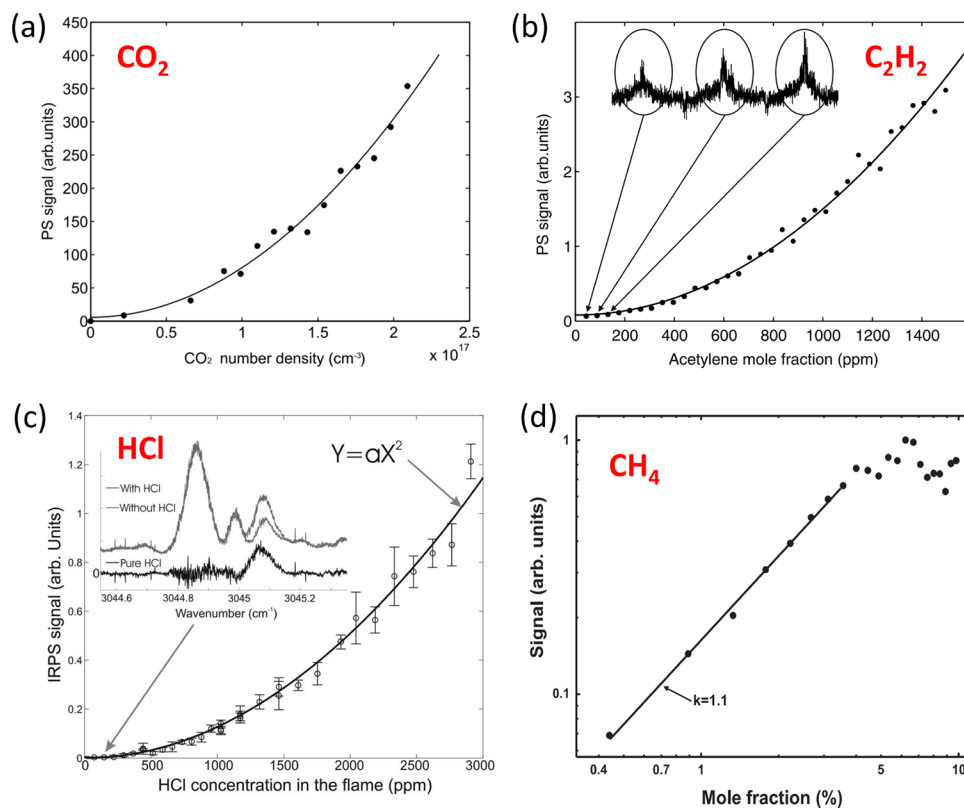

Fig. 5 Short IRPS scans near the absorption frequency of C_2H_2 P(11), namely at 3255.5615 cm^{-1}. Each scan was recorded with a binary mixture of C_2H_2 and Kr. In each scan, the C_2H_2 pressure was kept constant at 74.5 mTorr and the Kr pressure was increased from 6 to 130 Torr. [45]

not easy to decouple the temperature from the overlapping integral of the IR laser spectral profile with the IR absorption profile of each transition. This may be resolved by wavelength scanning for each transition and using the integrated line intensity to extract the gas temperature, based on the two-line ratio.

In addition, the measurement accuracy is always constrained by the low molecular number density, which may further contribute to a low S/N ratio. According to

Sahlberg et al. [16], when using H_2O line ratios, a total uncertainty of ± 100 K was estimated for the $CH_4/O_2/N_2$ flame at 2250 K. While ± 50 K uncertainty is caused by the standard deviation of different scans, another 50% of the uncertainty is due to the simulated line ratio at 1000 K and the accuracy of the calibration points. In addition, the heat loss to the burner and surrounding air also contributes to the higher simulated flame temperature compared to the measured temperature in the experiment.

5 Future prospects

The application of IRPS has attracted significant attention in quantitative measurements of combustion species and temperatures.

The unique feature of IRPS fills the gap of the absence of quantitative laser diagnostics tools suitable for reactive flows especially those with particulates. As such, it can be used to detect species and temperature needed for the understanding of current problems with the existing fossil-based flames. It also has the potential to be the tool of choice to study flames or newly adopted alternative fuels such as NH_3 and H_2 in the future. In particular, IRPS will the quantitative detection of key radicals such as NH and OH simultaneously with gas temperature. The P and R transitions in NH $(0-1)(X^3\Sigma^-)$ and OH $(0-1)(X^2\Pi)$ bands,

(a)

Fig. 7 Illustration of vibrational transitions of various molecules with corresponding intensity and typical frequency range for the IRPS detection [48]
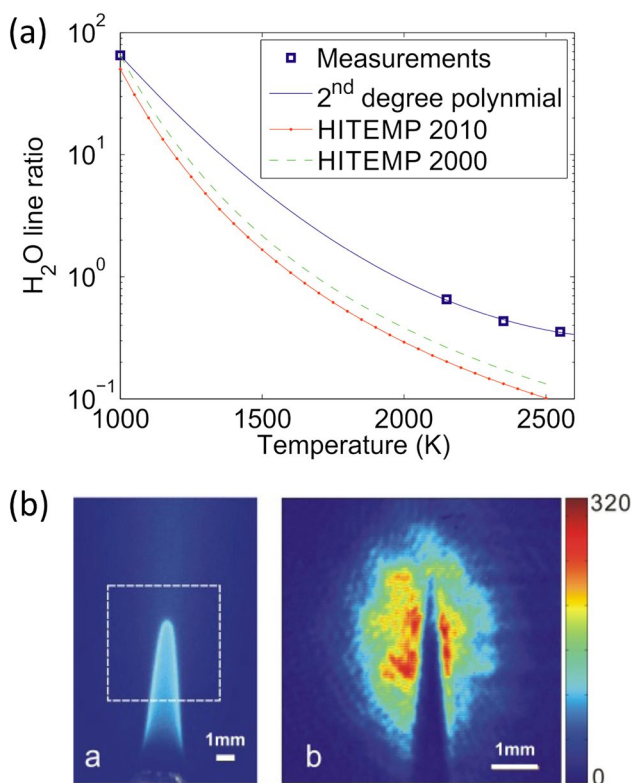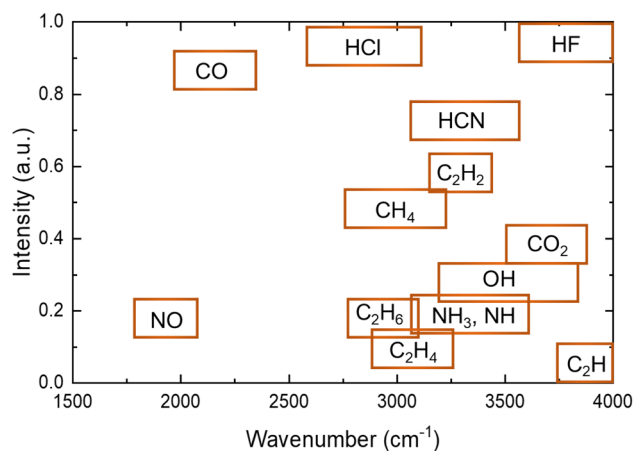
(b)

Fig. 6 a Comparison of the H_2O line ratio between the measurements and simulations using HITEMP 2010 and 2000. Reproduced from ref. [16] with permission. Copyright 2019 SAGE. **b** Images of the CH_4/O_2 Bunsen flame (left) and the single shot of HF (right) using two-dimensional IRPS. Reproduced from ref. [46] with permission. Copyright 2015 The Optical Society

near 3500 cm^{-1}, are readily accessible using difference-frequency generation in $LiNbO_3$ crystal. As the detection is linked to the electronic ground state, the issue of collisional quenching is minimized. The other challenging issue that remains is the dephasing collisions and collisional broadening. However, a recent study has shown that the coefficients of the collisional relaxation phenological rates for C_2H_2 with N_2 and CO_2 differ by ~ 19% [45]. In other words, there is no need to identify the mixture fraction for the entire composition to convert the signal into a quantitative concentration, which simplifies the process significantly. More importantly, molecules that do not fluoresce (usually termed dark molecules), can also be detected using IRPS. For example, the concentration of C_2H in hydrocarbon flames can be recorded using the IRPS technique by probing the low-lying electronic transition at ~ 3768 cm^{-1} [47].

Future progress in this field may involve further technical improvements. For example, the accuracy of the IRPS signal could be improved by the application of a single-mode laser with a high-quality beam profile. The

high-resolution spectra and pointing stability of such a laser make it feasible to improve the accuracy of the mole fractions and line ratios [16, 39]. As the transitions from 1 to 5.3 µm wavelength are important, the manufacture of a high-sensitive detector, such as indium-antimonide (InSb), in this range is necessary to improve the S/N ratio and is critical for the identification of minor species with low concentration. In addition, because the collision effect at low pressure is less severe, IRPS will be more suitable to study low-pressure flames rather than under atmospheric or high-pressure c onditions. Fur thermore, with accurate spectral simulation models, IRPS has the potential to perform sensitive detection of new species in flames.

For temperature measurement using IRPS, a more precise calibration between the temperature and line intensity ratio is required as well as the investigation of how these change under different pressures. Moreover, while the accuracy of temperature measurements is always constrained by the low molecular number density, which may furthe r contribute to a low S/N ratio, H_2O can provide the spectra with a high S/N ratio in low-pressure flames. Therefore, the application of IRPS in such flames will be attractive. The relationship between the changes in line intensity ratios and the changes in temperature and pressure could also be further investigated in temperature meas urements. Although IRPS has not been applied widely yet, this technique can be expected to become a common tool for concentration and temperature measurement not only in flames but also in other reaction-related environments, such as plasma [46].

6 Summary and conclusion

In this work, the development and application of IRPS have been reviewed for the quantitative measurements of combustion species and temperature. As many important combustion species, such as CO_2, C_2H_2, and CH_4, do not have accessible single-photon electronic transitions in the UV and visible spectral region, IRPS provides a solution to detect such species in the mid-IR region. Figure 7 summarizes the vibrational transitions of various molecules with corresponding intensity and typical frequency range. The molecules have infrared-active vibrational transitions with relatively high transition intensity, which makes them well suited for detection in the mid-IR range.

Compared with other nonlinear laser techniques, IRPS has the advantage of high intensity, enhanced S/N ratio, and low spectral interference from the IR radiation generated by the flame. Furthermore, it has the ability to perform in situ and non-intrusive measurements with high temporal and spatial resolution.

The theory, essential to understand IRPS and simulate the signal intensity and spectra, has been introduced in this review. A typical example of the simulated IRPS spectrum validates the feasibility of the numerical analysis. The specific lines can be selectively enhanced to identify and evaluate the target species in the experiment. Research published and achievements reported on the detection of combustion species employing IR polarization spectroscopy have also been summarized. In addition to the measurement of species concentrations and temperature, IRPS can also be used to study molecular dynamics and collision energy transfer. In contrast to other coherent techniques, its application can be further extended to the planar measurement for 2D imaging. The fast development and the availability of quantum cascade lasers will provide reliable and cost-effective mid-IR laser sources at wide mid-IR wavelength sources [31]. This will help the further development of IRPS in the near future. It is concluded that IRPS is a promising diagnostic method for the measurement of infrared active species in both particle-free flames and particle-laden environments, in cluding the study of gaseous molecular spectroscopy.

Declarations

References

1. C. Wieman, T.W. Hänsch, Doppler-Free Laser Polarization Spectroscopy. Phys. Rev. Lett. **36**(20), 1170–1173 (1976)
2. R.L. Farrow, R.P. Lucht, W.L. Flower, R.E. Palmer, Coherent anti-stokes raman spectroscopic measurements of temperature and acetylene spectra in a sooting diffusion flame: Colloquium on combustion diagnostics. Sympos. Int. Combus. **20**(1), 1307–1312 (1985)
3. K. Nyholm, Measurements of OH rotational temperatures in flames by using polarization spectroscopy. Opt. Commun. **111**(1–2), 66–70 (1994)
4. J. Reppel, Z.T. Alwahabi, Orthogonal planar laser polarization spectroscopy. Appl. Opt. **41**(21), 4267–4272 (2002)
5. T.A. Reichardt, F. Di Teodoro, R.L. Farrow, S. Roy, R.P. Lucht, Collisional dependence of polarization spectroscopy with a picosecond laser. J. Chem. Phys. **113**(6), 2263–2269 (2000)
6. J. Walewski, M. Rupinski, H. Bladh, Z.S. Li, P.E. Bengtsson, M. Aldén, Soot visualisation by use of laser-induced soot vapourisation in combination with polarisation spectroscopy. Appl. Phys. B **77**(4), 447–454 (2003)
7. K. Nyholm, M. Kaivola, C.G. Aminoff, Polarization spectroscopy applied to C2 detection in a flame. Appl. Phys. B **60**(1), 5–10 (1995)
8. A.A. Suvernev, A. Dreizler, T. Dreier, J. Wolfrum, Polarization-spectroscopic measurement and spectral simulation of OH ($A^2\Sigma$-$X^2\Pi$) and NH ($A^3\Pi$-$X^3\Sigma$) transitions in atmospheric pressure flames. Appl. Phys. B: Lasers Opt. **61**(5), 421–427 (1995)
9. B. Lofstedt, R. Fritzon, M. Aledn, Investigation of NO detection in flames by the use of polarization spectroscopy. Appl. Opt. **35**(12), 2140–2146 (1996)
10. T. Dreier, P. Ewart, Coherent Techniques for Measurements with Intermediate Concentrations, in *Applied Combustion Diagnostics*. ed. by K. Kohse-Höinghaus, J. Jeffries (Taylor & Francis, London, 2002), pp.69–97
11. S. Roy, R.P. Lucht, A. McIlroy, Mid-infrared polarization spectroscopy of carbon dioxide. Appl. Phys. B: Lasers Opt. **75**(8), 875–882 (2002)
12. Z.T. Alwahabi, Z.S. Li, J. Zetterberg, M. Aldén, Infrared polarization spectroscopy of CO2 at atmospheric pressure. Opt. Commun. **233**(4–6), 373–381 (2004)

13. M. Aldén, J. Bood, Z. Li, M. Richter, Visualization and understanding of combustion processes using spatially and temporally resolved laser diagnostic techniques. Proc. Combust. Inst. **33**(1), 69–97 (2011)

14. Z.S. Li, M. Rupinski, J. Zetterberg, Z.T. Alwahabi, M. Aldén, Mid-infrared polarization spectroscopy of polyatomic molecules: Detection of nascent CO2 and H2O in atmospheric pressure flames. Chem. Phys. Lett. **407**(4–6), 243–248 (2005)

15. Z.S. Li, C. Hu, J. Zetterberg, M. Linvin, M. Alden, Midinfrared polarization spectroscopy of OH and hot water in low pressure lean premixed flames. J. Chem. Phys. **127**(8), 084310 (2007)

16. A.L. Sahlberg, D. Hot, R. Lyngbye-Pedersen, J. Zhou, M. Alden, Z. Li, Mid-infrared polarization spectroscopy measurements of species concentrations and temperature in a low-pressure flame. Appl. Spectrosc. **73**(6), 653–664 (2019)

17. J. Kiefer, P. Ewart, Laser diagnostics and minor species detection in combustion using resonant four-wave mixing. Prog. Energy Combust. Sci. **37**(5), 525–564 (2011)

18. S. Cheskis, A. Goldman, Laser diagnostics of trace species in low-pressure flat flame. Prog. Energy Combust. Sci. **35**(4), 365–382 (2009)

19. Demtröder, W., *Laser spectroscopy: Vol. 2: Experimental Techniques*. Springer: 2008; Vol. 2.

20. Teets, R.; Kowalski, F.; Hill, W.; Carlson, N.; Hansch, T., *Laser Polarization Spectroscopy*. SPIE: 1977; Vol. 0113.

21. Z.S. Li, M. Linvin, J. Zetterberg, J. Kiefer, M. Aldén, Mid-infrared polarization spectroscopy of C2H2: non-intrusive spatial-resolved measurements of polyatomic hydrocarbon molecules for combustion diagnostics. Proc. Combust. Inst. **31**(1), 817–824 (2007)

22. T.A. Reichardt, W.C. Giancola, R.P. Lucht, Experimental investigation of saturated polarization spectroscopy for quantitative concentration measurements. Appl. Opt. **39**(12), 2002–2008 (2000)

23. T.A. Reichardt, R.P. Lucht, Theoretical calculation of line shapes and saturation effects in polarization spectroscopy. J. Chem. Phys. **109**(14), 5830–5843 (1998)

24. Z.W. Sun, Z.S. Li, B. Li, Z.T. Alwahabi, M. Aldén, Quantitative C2H2 measurements in sooty flames using mid-infrared polarization spectroscopy. Appl. Phys. B **101**(1–2), 423–432 (2010)

25. Z.T. Alwahabi, J. Zetterberg, Z.S. Li, M. Aldén, High resolution polarization spectroscopy and laser induced fluorescence of CO2 around 2μm. Eur. Phys. J. D **42**(1), 41–47 (2006)

26. Banwell, C. N., *Fundamentals of molecular spectroscopy*. Tata McGraw-Hill Publishing Company: (1983)

27. Z.T. Alwahabi, J. Zetterberg, Z.S. Li, M. Aldén, Measurements of Collisional Broadening Coefficients by Infrared Polarization Spectroscopy. Appl. Spectrosc. **61**(4), 424–427 (2007)

28. R.W. Parsons, V.I. Metchnik, R.J. Dyne, The Collision Broadening of Spectral Lines. Aust. J. Phys. **21**(1), 13–20 (1968)

29. D. Jacquemart, J.Y. Mandin, V. Dana, C. Claveau, J. Vander Auwera, M. Herman, L.S. Rothman, L. Régalia-Jarlot, A. Barbe, The IR acetylene spectrum in HITRAN: update and new results. J. Quant. Spectrosc. Radiat. Transfer **82**(1–4), 363–382 (2003)

30. M. Šimečková, D. Jacquemart, L.S. Rothman, R.R. Gamache, A. Goldman, Einstein A-coefficients and statistical weights for molecular absorption transitions in the HITRAN database. J. Quant. Spectrosc. Radiat. Transfer **98**(1), 130–155 (2006)

31. Razeghi, M.; Bandyopadhyay, N.; Bai, Y.; Lu, Q.; Slivken, S., Recent advances in mid infrared (3–5μm) Quantum Cascade Lasers. Opt. Mater. Express *3* (11) (2013)

32. Bartalini, S.; Borri, S.; Natale, P. D., Doppler-free polarization spectroscopy with a quantum cascade laser at 4.3 μm. Opt. Express 17 (9), 7440–7449 (2009)

33. Z.S. Li, M. Rupinski, J. Zetterberg, M. Aldén, Mid-infrared PS and LIF detection of CH4 and C2H6 in cold flows and flames at atmospheric pressure. Proc. Combust. Inst. **30**(1), 1629–1636 (2005)

34. Z.S. Li, Z.W. Sun, B. Li, M. Aldén, M. Försth, Spatially resolved trace detection of HCl in flames with mid-infrared polarization spectroscopy. Opt. Lett. **33**(16), 1836–1838 (2008)

35. J. Reppel, Z.T. Alwahabi, A uniaxial gas model of the geometrical dependence of polarization spectroscopy. J. Phys. D Appl. Phys. **34**(17), 2670–2678 (2001)

36. R. Teets, R. Feinberg, T.W. Hänsch, A.L. Schawlow, Simplification of spectra by polarization labeling. Phys. Rev. Lett. **37**(11), 683–686 (1976)

37. O. Lucas, Z.T. Alwahabi, V. Linton, K. Meeuwissen, Laser diagnostics of welding plasma by polarization spectroscopy. Appl. Spectrosc. **61**(5), 565–569 (2007)

38. Z.S. Li, M. Rupinski, J. Zetterberg, Z.T. Alwahabi, M. Aldén, Detection of methane with mid-infrared polarization spectroscopy. Appl. Phys. B **79**(2), 135–138 (2004)

39. K. Richard, P. Ewart, High-resolution infrared polarization spectroscopy and degenerate four wave mixing spectroscopy of methane. Appl. Phys. B **94**(4), 715–723 (2009)

40. Z.W. Sun, Z.S. Li, A.A. Konnov, M. Aldén, Quantitative HCN measurements in CH4/N2O/O2/N2 flames using mid-infrared polarization spectroscopy. Combust. Flame **158**(10), 1898–1904 (2011)

41. Z. Sun, M. Försth, Z. Li, B. Li, M. Alden, In situ Measurements of HCN in a tube furnace with infrared polarization spectroscopy. Fire Safety Sci. **10**, 279–291 (2011)

42. R.L. Pedersen, D. Hot, Z. Li, Comparison of an InSb detector and upconversion detector for infrared polarization spectroscopy. Appl. Spectrosc. **72**(5), 793–797 (2018)

43. Z.W. Sun, M. Försth, Z.S. Li, B. Li, M. Aldén, Mid-infrared polarization spectroscopy: a tool for in situ measurements of toxic gases in smoke-laden environments. Fire Mater. **35**(8), 527–537 (2011)

44. X. Chen, B.D. Patterson, T.B. Settersten, Time-domain investigation of OH ground-state energy transfer using picosecond two-color polarization spectroscopy. Chem. Phys. Lett. **388**(4–6), 358–362 (2004)

45. Alwahabi, Z. T.; Hu, C.; McCaffery, A. J.; Li, Z. S.; Aldén, M., Collisional Relaxation in Infrared Polarisation Spectroscopy. Unpublished results.

46. Z. Sun, J. Zetterberg, Z. Alwahabi, M. Alden, Z. Li, Single-shot, planar infrared imaging in flames using polarization spectroscopy. Opt Express **23**(23), 30414–30420 (2015)

47. E.N. Sharp-Williams, M.A. Roberts, D.J. Nesbitt, High resolution slit-jet infrared spectroscopy of ethynyl radical: $^2\Pi$–$^2\Sigma^+$ vibronic bands with sub-Doppler resolution. J Chem Phys **134**(6), 064314 (2011)

48. L.S. Rothman, I.E. Gordon, Y. Babikov, A. Barbe, D. Chris Benner, P.F. Bernath, M. Birk, L. Bizzocchi, V. Boudon, L.R. Brown, A. Campargue, K. Chance, E.A. Cohen, L.H. Coudert, V.M. Devi, B.J. Drouin, A. Fayt, J.M. Flaud, R.R. Gamache, J.J. Harrison, J.M. Hartmann, C. Hill, J.T. Hodges, D. Jacquemart, A. Jolly, J. Lamouroux, R.J. Le Roy, G. Li, D.A. Long, O.M. Lyulin, C.J. Mackie, S.T. Massie, S. Mikhailenko, H.S.P. Müller, O.V. Naumenko, A.V. Nikitin, I. Orphal, V. Perevalov, A. Perrin, E.R. Polovtseva, C. Richard, M.A.H. Smith, E. Starikova, K. Sung, S. Tashkun, J. Tennyson, G.C. Toon, V.G. Tyuterev, G. Wagner, The HITRAN2012 molecular spectroscopic database. J. Quant. Spectrosc. Radiat. Transfer **130**, 4–50 (2013)